Origin of high- and low-conductance traces in alkanediisothiocyanate single-molecule contacts

D. A. Luzhbin[1,2,*] and C.-C. Kaun[1,†]
[1]*Research Center for Applied Sciences, Academia Sinica, Taipei, Taiwan*
[2]*G. V. Kurdyumov Institute for Metal Physics, Kyiv, Ukraine*
(Received 24 May 2009; revised manuscript received 24 July 2009; published 25 January 2010)

Zero-bias transport properties of alkanediisothiocyanate [-SCN-$(CH_2)_n$-NCS-, $n=4,6,8$] molecules anchored to various quasi-one-dimensional Au(111) electrodes are studied by an *ab initio* method within a standard two-probe methodology based on the density-functional theory and the nonequilibrium Green's functions formalism. We have shown that the high-/low-conductance traces observed in STM break-junction experiments on this molecular species can be clearly related to the difference in the electronic structures between the molecular contacts with different geometric configurations of the near-interface planes of the electrodes. The difference in transport properties of alkanediisothiocyanate single-molecule junctions can be understood in terms of the distribution of the surface states, emerging in the energy gap of the alkanes due to the electrode environment. A general feature of the high-conductance junctions is a number of closely located surface states around the Fermi energy, well coupled to the scattering states of the junctions. These well-coupled states broaden the transmission peaks responsible for conductance, increasing their amplitudes at the Fermi energy, while the sparser distribution of the surface states gives sharper peaks with smaller amplitudes at the Fermi energy, naturally representing the low-conductance junctions. The effects of changing the end groups, junction distance, and electrode cross-section are also investigated and analyzed in terms of changes in the electronic structure of the molecular junctions. A comparison with the available experimental data is also provided.

DOI: 10.1103/PhysRevB.81.035424 PACS number(s): 73.63.−b, 85.65.+h, 73.40.−c, 73.23.Ad

I. INTRODUCTION

Progress in controllable formation of single-molecule contacts (SMCs) and consistent measurement of their electrical properties,[1–3] accompanied by a rapid development of efficient numerical tools for quantum-mechanical *ab initio* analysis[4–7] of transport properties of SMCs, achieved in the last decade, has spawned a large number of works studying various aspects of quantum transport in nanoscale molecular devices, particularly in view of their potential application in the field of molecular electronics.[3,8]

A numerical *ab initio* approach based on combination of the real-space density-functional theory and the nonequilibrium Green's functions formalism (DFT-NEGF) (Refs. 4–7) has turned out to be one of the most widely used methods nowadays, giving accurate results on the transport properties of SMCs,[9–11] magnetic tunnel junctions,[12] atomic clusters,[13] self-organized carbon structures,[14,15] etc.

Despite significant progress toward the understanding of transport properties of SMCs from the first principles, for a number of molecules, the calculated conductance was found to be more than an order of magnitude larger than the experimental value.[11,16] A number of other effects such as electromechanic, electrostatic, and stochastic current switching (observed in π-conjugated systems and alkanethiols), conductance fluctuations,[17–19] (4–5)-fold separation between the high-conductance (HC) and the low-conductance (LC) traces observed in STM break-junction experiments,[20–23] etc., still awaits unified view on their origin despite a number of plausible explanations already proposed.[17–21,24]

Owing to their stability, thiol-terminated organic molecules bridging gold electrodes have been attractive systems for investigating quantum transport in molecular junctions and are widely considered as a kind of model system for theoretical studies.[9,16,25] Among those, alkanethiol molecules, able to form prototypical self-assembled monolayers on gold surfaces, have been subjected to intensive experimental[2,18,20,21,23,26] and theoretical[9,17,20,27,28] studies, with a rather good agreement between the experimental and the *ab initio* numerical data.[9,11,17]

It has been theoretically[9,29–31] and experimentally[22,23,32,33] shown that changing the end groups in an SMC can considerably change its transport properties. With isothiocyanates substituted for thiols, the resistance of alkanediisothiocyanate (ADTC) SMCs significantly increases compared to that of alkanedithiol SMCs as experimentally observed in Ref. 23. ADTC molecular contacts also reveal two profiles in their conductance histograms, namely, the HC and LC ones, with their ratio of about 8–10 for different alkanes. As for the alkanedithiol SMCs, the appearance of the HC and LC traces is usually attributed either to different binding sites of the sulfur end groups[20,21] or to the details of the atomic configuration at the molecule-metal interface.[27] However, bonding of isothiocyanates to Au surfaces is different from that of thiols,[34,35] thus the origin of the two conductance traces obtained in the ADTC SMCs requires further investigation.

In this paper we numerically investigate the dependence of the zero-bias transmission spectra of alkanediisothiocyanate single-molecule contacts on the geometrical configuration of two quasi-one-dimensional gold electrodes. Given the fact that theoretical study of ADTC SMCs has thus far received much less attention than its alkanethiol counterpart, it is important to address the question of general peculiarities of quantum transport through ADTC SMCs as well as the question of origin of the HC/LC separation in this species. We have proposed a rationale that gives the HC/LC separation value and the occurrence ratio of the HC/LC sets very close to those observed experimentally. The experimental

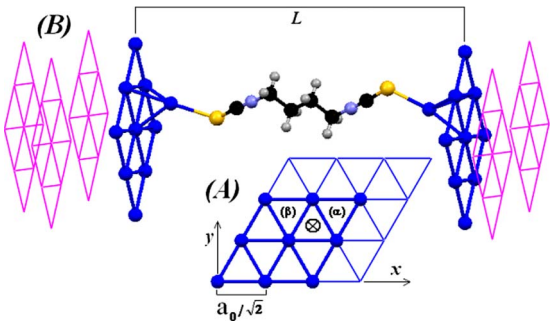

FIG. 1. (Color online) (a) (Bold lines) A (2×2) slice used for constructing an Au(111) quasi-one-dimensional infinite electrode. (Thin lines) A (3×3) slice for the electrode with a larger cross-sectional area used for comparison. ⊗ marks the binding site (top view) of the Au adatoms. (b) Geometric configuration of the scattering region for a butane SMC. For clarity, no bonds between the slices are shown. L is the interelectrode distance along the transport direction measured between the fixed terminal electrode slices. Shown in bold is the geometric setup used for structural relaxation.

data of Fu *et al.*[23] are used for comparison with our numerical results.

II. COMPUTATIONAL SETUP

A. Formation of a molecular junction

It has been observed[36] that during the repetitive STM break-junction measurements narrow filaments of gold are pulled out of the gold surface, thus justifying the use of the one-dimensional electrodes rather than planar or bulk geometry. Molecular-dynamics simulations,[37] *ab initio* calculations,[38] and experimental data[39] favor the formation of gold nanowires in (111) direction and preferable adsorption of molecules on (111) surface, thus giving us a hint of how the contact geometry can be modeled.

A basic unit for constructing an electrode with a finite cross-sectional area is a slice made up of nine Au atoms as shown in Fig. 1(A) with the interatomic distances corresponding to those of the bulk material. A unit cell of the quasi-one-dimensional (111) electrode used in our calculation is formed by subsequent shifts of the basic slice onto $d=a_0/\sqrt{3}$ along z direction (perpendicular to its plane; a_0 is the length of the fcc unit cell of bulk gold and is equal to 4.08 Å throughout the calculations) and onto the translation vector $\vec{T}_{n_2}$ within its plane, with the x and y components of $\vec{T}_{n_2}$ being the real and imaginary parts of $a_0\exp[i(1+2n_2)\pi/6]/\sqrt{6}$ $(n_2=0,1,\ldots,5)$, respectively, and subsequent shifts of the next slice (with respect to the previous one) onto d along z direction and corresponding vector $\vec{T}_{n_3}$ within its plane. After that, the unit cell containing three slices is periodically repeated along z direction with the period $3d$. To match the (111) geometry, pairs (n_2,n_3) must be either odd-odd or even-even, so only 18 different permutations are possible. In what follows we will refer to any of these structures simply by giving their indices, e.g., 24 is the structure with $n_2=2$ and $n_3=4$.

Molecular junctions used in our study are formed of n-alkanediisothiocyanates [-SCN-$(CH_2)_n$-NCS-] $(n=4,6,8)$ placed between two Au(111) electrodes with an Au adatom from each side [Fig. 1(B)], a geometry that is likely to occur at break junctions for SMCs with thiol (-S-)(Ref. 21) or amine (-NH_2-) (Ref. 33) end groups. For the geometry relaxation, the molecules were placed between the two symmetric Au slices with one Au adatom from each side as shown in bold in Fig. 1(B). Having fixed positions of all Au atoms in the slice planes, all other atoms were relaxed using the GAUSSIAN-03 software[40] (at DFT level of theory, with B3PW91 functional and LANL2DZ basis set for all the elements; singlet ground state was assumed) until the residual forces acting on every atom were <0.037 nN. Having relaxed the structure, the right gold slice was shifted along z axis onto a distance $\Delta L=0.05$ Å (the molecule with Au adatoms was shifted onto $\Delta L/2$) and optimization was performed once again. Since no thermal fluctuations are included into the computation model, this stretching algorithm corresponds to the adiabatic stretching regime.[18] All relaxed structures for each value of the interelectrode separation L were used for subsequent transport calculation.

During the initial relaxation the binding site of the Au adatoms was found to lie above the hollow site of the inner triangle of the slice, as shown in Fig. 1(A), giving the minimal total energy of the whole system. The same preferential binding site was also found for pure thiocyanate molecules.[34] We have found that with increasing the interelectrode separation, the most energetically favorable binding site for the Au adatoms remains within this triangle. If not mentioned otherwise, all the results reported in the present work are for this preferential binding site.

Our choice of the (111) structure formation gives us essentially three different electrodes with different band structures. These electrodes are represented by configurations 00,33 (group I), 11,22,44,55 (group II), and 02,04,13,15,20,24,31,35,40,42,51,53 (group III), with all the structures within each group representing the same (up to a mirror reflection, which does not change the electrode band structure) infinite electrode. However, terminating the infinite electrode with a molecular contact breaks the symmetry and every given (n_2,n_3) geometry within the two-probe setup is different from the others in terms of its near-interface structure, where the screening takes place, which is mostly determined by the first two layers of gold atoms.[5,41]

The two-probe setup for the calculation has been organized as follows. The stacking of the infinite electrode in the transport direction follows the …ABCABC… pattern. The lead unit cell is built of three gold slices that follow CAB pattern. The scattering region is built of four gold slices from the left side that follow CABC pattern, where A is the basic slice located at $z=d$, with B and C being the properly shifted slices, the molecule with the end groups, and three gold slices from the right side that follow CAB pattern, see Fig. 1(B). As shown in Ref. 5 and as we have verified throughout our calculations this choice of the two-probe structure provides smooth match of the equilibrium charge density across the boundaries between the scattering region and the electrodes.

It should also be noted that the electrodes with $n_2=n_3$ are highly unstable because they involve incompact structures

with dangling atoms only connected to a couple of atoms in the same slice, and with the C-A slices being connected through less than the half of their surfaces, thus being very prone to relaxation into more compact structures with lower energy. As our calculation shows, the total energy of the scattering region of the two-probe systems that belong to the group I(II) is about 8(25) eV higher than that of the group-III configurations, suggesting that formation of the groups I and II in an experiment is much less probable. Taking that into account, hereafter we concentrate on the analysis of the molecular configurations of the group III, and results for the unstable groups I and II will be presented only for the sake of completeness.

The present work is limited to the case of the symmetric structures with the two terminal Au slices having the same x and y coordinates and being only shifted onto L along z direction, and with the same stacking of the left and the right electrodes ($n_i^l = n_i^r$, $i=2,3,r,l$ indices refer to the right and the left electrodes, respectively). The more comprehensive analysis of the general case of different stacking of the left and the right electrodes ($n_i^l \neq n_i^r$) as well as the case of the left and the right electrodes being shifted with respect to each other within the x-y plane will be reported elsewhere.

B. Computational details

The DFT-NEGF *ab initio* technique used in our work has been implemented in MATDCAL software, with all the technicalities and mathematics documented in Refs. 4 and 12. All the results shown in this work are for double-ζ linear combination of atomic orbitals basis set for s, p, and d electrons in the active space, with core electrons represented by standard nonlocal norm-conserving pseudopotentials,[42] and the local-density approximation in Perdew-Zunger parametrization[43] for the exchange-correlation functional. We have also checked that the use of a double-ζ-polarized basis set and/or the general-gradient approximation in Perdew-Burke-Ernzerhof (PBE) parametrization[44] for the exchange-correlation functional, using a similar DFT-NEGF algorithm implemented in ATK-2.3.2 suite of programs,[5] gives essentially the same results.

The periodic boundary conditions are imposed on the x-y plane with the primitive vectors $(5.2\times a_0, 0)$ and $(0, 5.2\times a_0)$, and only the Γ point in the transverse momentum plane and a mesh of 600 equidistant k points along the transport direction is used for the electronic structure calculations. We have tested the change in the gap size by increasing the cell size from $5.2\times a_0$ to $8\times a_0$ and found only negligible changes.

III. RESULTS AND DISCUSSION

With increasing the distance L between the terminal Au slices, at certain distances, the molecular contacts break from one side[45] during the relaxation. We have found the following maximum distances for which molecules still form contact with both electrodes: $L_c=21.1$ Å for butane, $L_c=23.675$ Å for hexane, and $L_c=26.29$ Å for octane (a finer than 0.05 Å step size was used around the breakage distances). Hereafter, if not mentioned otherwise, all reported figures are for these critical values of the interelectrode separation.

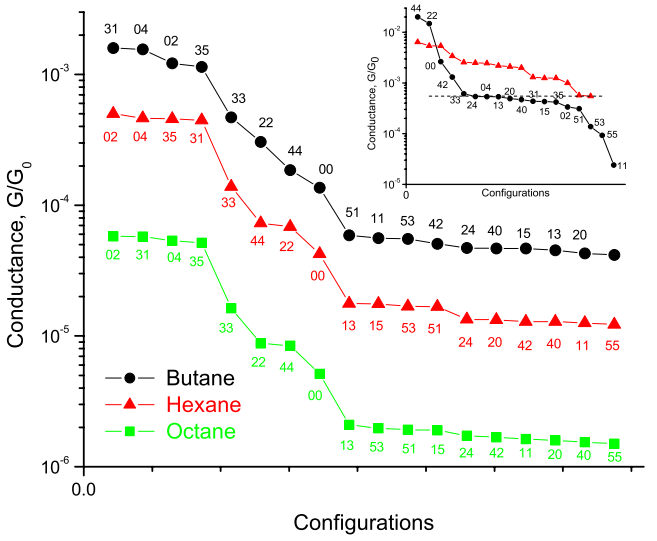

FIG. 2. (Color online) Zero-bias conductance values (in units of the conductance quantum) for all studied [-SCN-$(CH_2)_n$-NCS-] ($n=4,6,8$) molecular junctions. Two distinct conductance values are clearly seen with values represented by the unstable configurations 00,22,33,44 lying in between. (Inset) Sorted distribution of conductance values for a hexane dithiol molecular contact for the same molecular binding site (Ref. 52) (circles) together with the numerical data adopted from Ref. 27 (triangles) (Ref. 53). Conductance of an SMC (from Ref. 27) with the molecule-electrode interface geometry similar to one used in the present work is marked with a horizontal dashed line. In what follows the marks in colors correspond to the curves of the same colors.

Figure 2 shows the values of the zero-bias conductance (sorted in descending order) for all studied configurations. One clearly sees two groups of conductance values that differ of about an order of magnitude, with the high-conductance values represented by configurations 02,04,31,35, and the low-conductance values represented by configurations 13,15,20,24,40,42,51,53, while some of the unstable configurations give conductance either in between the HC and LC regions (00,22,33,44) or in the LC (11,55) region.

Another interesting trend revealed in our calculation is the grouping of the zero-bias transmission spectra $T(E)$ and the density of states (DOS) curves. As shown in Fig. 3(A) HC configurations 02,04,31,35 all have the similar dependence of the transmission coefficient on the incident electron energy, $T(E)$, and the same is for two LC quartets built of configurations 13,24,42,53 [Fig. 3(B)] and 15,20,40,51 [Fig. 3(C)]. $T(E)$ dependences of the unstable configurations group as follows: 11–55, 22–44, whereas 00 and 33 do not correlate with any other dependences [Figs. 3(D)–3(F)]. The same trend applies to the DOS vs E dependences.

In order to further elucidate the appearance of the HC and LC values, in Fig. 4 we plot the dependence of the conductance of a butane SMC as a function of the interelectrode distance L, see Fig. 1(B). The molecular junction breaks at the distance $L > L_c = 21.1$ Å, and further increase in the in-

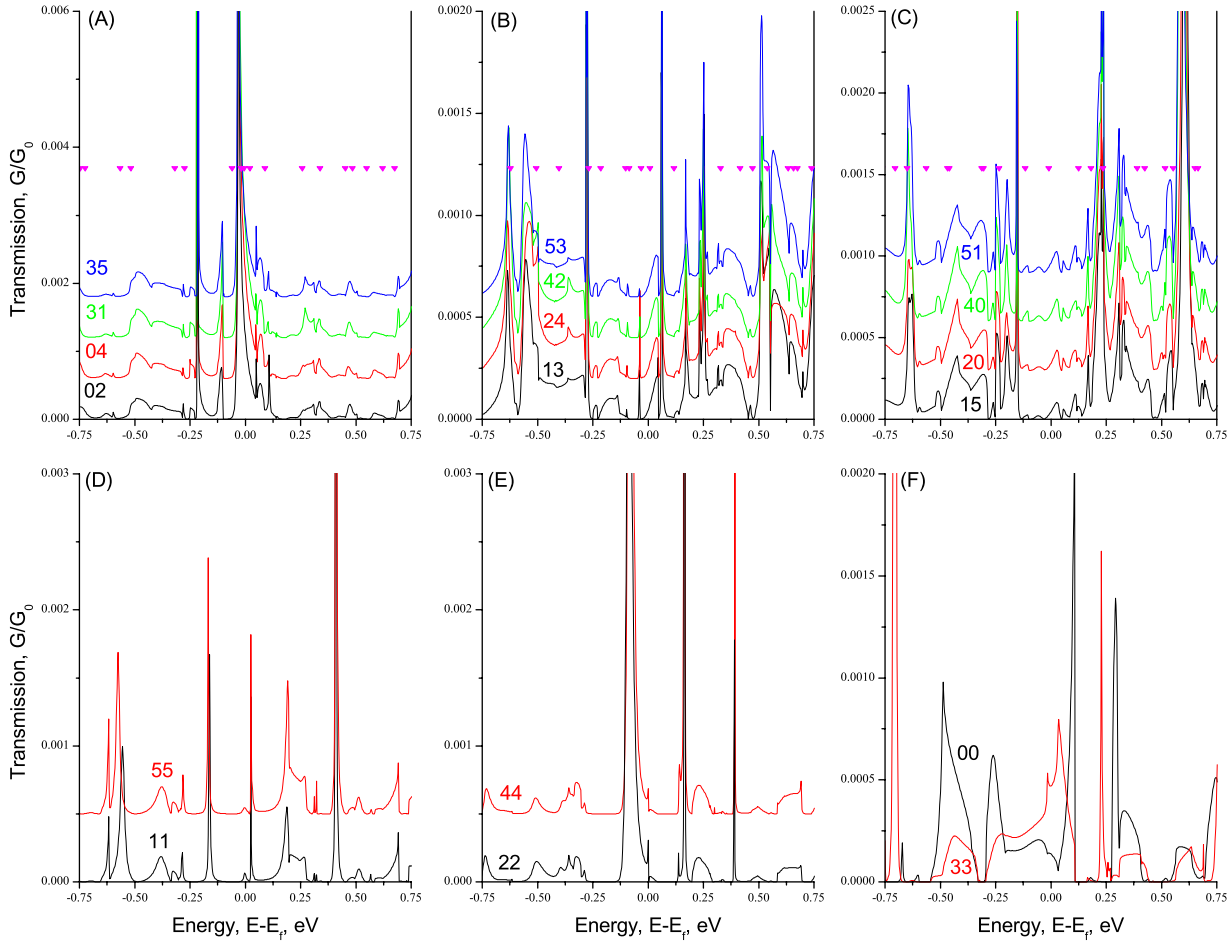

FIG. 3. (Color online) Transmission spectra for all studied SMC configurations for a butane SMC. Filled triangles in (A)–(C) show positions of the renormalized molecular levels of the Hamiltonian associated with all the atoms in the scattering region. For clarity, the curves are shifted along the axis of ordinates, each one with respect to the lower one onto (A) $0.0006 \times G_0$, (B) $0.0002 \times G_0$, (C) $0.0003 \times G_0$, and (D) and (E) $0.0005 \times G_0$. No shift in (F).

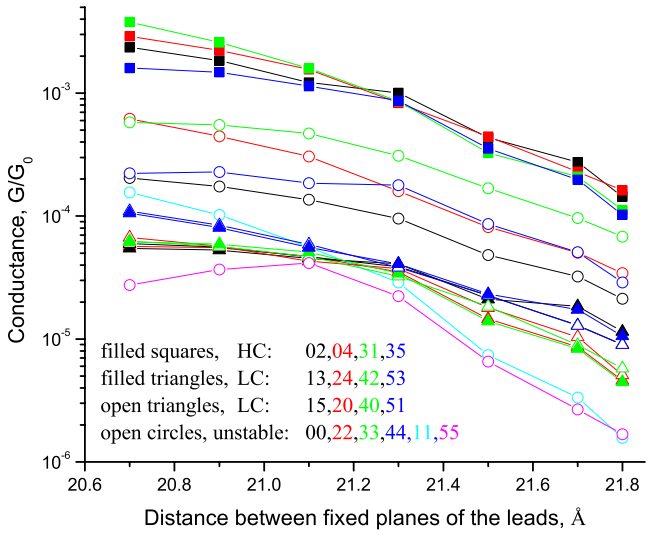

FIG. 4. (Color online) Length dependence of the conductance for a butane SMC with different configurations of the electrodes. The solid lines are guides for the eyes only.

terelectrode separation leads to a clear tunneling behavior with $G(L)$ depending linearly on L in a semilog scale. The HC/LC separation remains of the same order for all values of L suggesting that the origin of this separation is associated with only one of the electrodes (left in our case).

Figure 5 shows a semilog plot of the conductance versus the number of methylene units for all studied SMCs together with the experimental values.[23] Numerical values for the LC and HC regions match to those of the experiment, except for the slope of the curves: inward for experiment and outward for *ab initio*. The same slope has also been observed in our independent calculations with Au(100) electrodes. A possible origin of that backward sloping could lie in our choice of the junction breakage distance L_c (Ref. 45); as one can see in Fig. 4 a 0.4 Å increase in L results in up to five times decrease in conductance. Commonly used exponential interpolation[9,17,20–23,27,31,33] of the single-molecule resistance (which is the inverse of conductance) versus the number of methylene units n, $R=R_0 \exp(\beta_n n)$, gives the following average values for the tunneling decay constant β_n and the contact resistance R_0: $\beta_n=0.80\pm0.18$, $R_0=331$ kΩ for the HC and $\beta_n=0.83\pm0.18$, $R_0=8363$ kΩ for the LC groups, in very rough accordance with the experimental values[23]

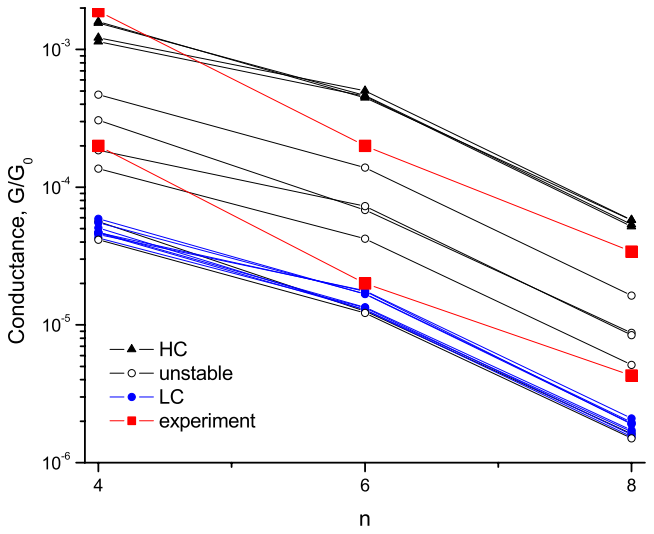

FIG. 5. (Color online) n dependence of the HC and LC conductance values for different configurations of the electrodes. Red bold squares represent experimental data (Ref. 23). Hollow circles corresponding to the unstable configurations 00,11,22,33,44,55 lie either in the gap between the HC and LC regions or in the LC region configurations 11,55).

$1.01 \pm 0.07/0.96 \pm 0.07$ for β_n and $128 \pm 59/1560 \pm 720$ kΩ for R_0 for the HC/LC, correspondingly. However, standard error form the least-squares approximation in a semilog scale gives uncertainty exceeding 100% in the average values of R_0.

Since the main source of disagreement between the experimental and the calculated values of β_n is the poor performance of the least-square approximation, we will proceed with establishing a general trend that relates values of β_n in the HC and LC regions to each other. In a simple tunneling model[21,23,26,31] with a rectangular barrier $\beta_n=(\alpha\Phi_b)^{1/2}$, where α is some constant that includes the effective mass of the charge carriers and Φ_b is the potential barrier height, which we associate with the energy difference between the highest occupied molecular orbital (HOMO) energy level and the Fermi energy E_f of the electrodes, $\Phi_b=|E_f-E_{\mathrm{HOMO}}|$,[20,31] which equals 1.4 eV for the LC configurations. Self-consistent solution of the transport equations shows that there is a charge transfer at the metal-molecule interface, which is of about $-0.1e$ for the HC configurations (a negative charge transfer means that the molecule has lost electrons to the metal electrodes) and $+0.1e$ for the LC configurations, with e being the elementary charge. Due to this charge-transfer position of the HOMO for the HC junctions is shifted of about −0.1 eV with respect to that of the LC junctions. As one can show from simple algebra, $\beta_n^{\mathrm{HC}}=[\alpha(\Phi_b+0.1)]^{1/2}\approx\beta_n^{\mathrm{LC}}(1+0.04)$, where $\beta_n^{\mathrm{LC}}=(\alpha\Phi_b)^{1/2}$, which is in excellent agreement with the experimental results.[23] As shown in Ref. 31, within the tunnel barrier model, the value of β is sensitive to the alignment of the Fermi level within the molecular HOMO-lowest unoccupied molecular orbital (HOMO-LUMO) gap. Thus, changing the molecular binding site or the cross-sectional area of the electrodes could vary the barrier height Φ_b, thus changing the value of β_n^{LC} and giving more accurate agreement with the experiment. On the other hand, the disagreement between the experimental and the numerical values of β_n and R_0 can only be slightly reduced by increasing the accuracy of the basis set, while the difference in the curves' slope is insensitive to the basis set choice.

Comparison to alkanes terminated with amine[22,30–33] and thiol[9,17,20–22,27,31] end groups, which have recently attracted considerable interest, allows us to draw the following estimation. The HOMO-E_f offset for diisothiocyanate end groups, 1.4 eV, is smaller than reported 2.83 eV for diamines and 1.84 eV for dithiols,[31] thus suggesting that for SMCs with diisothiocyanate end groups β_n should be smaller than that for SMCs with diamine or dithiol end groups, in accordance with the published numerical results.[31] However, this disagree with the experimental findings[23] that give the value of β_n almost identical to that of dithiol SMCs. Among these end groups, diisothiocyanates form junctions with the highest contact resistance [cf. with numerical values $R_0^{diamine}=140$ kΩ,[30] $R_0^{dithiol}=1.5$ kΩ for Au(100) electrodes[9] and $R_0^{dithiol}=53.8$ kΩ for clusterlike Au electrodes[20]], in agreement with the experimental trend $R_0^{\mathrm{ADTC}}>R_0^{dithiol}$ (Ref. 23) and $R_0^{diamine}>R_0^{dithiol}$ (Ref. 22) for both the LC and HC sets.

The transport properties of SMCs are determined by the electronic structure of the combined molecule and electrodes system. With a molecule bridging the interelectrode gap, the transport through a two-probe system is determined by its scattering states $\phi^{SS}(E)$,[4,5] which are Bloch waves in the electrodes and molecularlike states in the scattering region. However, these states have different weights, some being localized on the contacts, some on the bridging molecule, and some delocalized over the whole scattering region. These scattering states correspond to transmission eigenchannels, which can numerically be obtained by the eigenvalue decomposition of the transmission amplitude matrix[46] or, independently, within the NEGF formalism.[47] The problem of calculating the scattering states is described in details in Refs. 5 and 47. The proper analysis shows that in all our ADTC SMCs there is only one conducting channel that corresponds to the mostly delocalized scattering-state wave function ϕ^{SS}.

General peculiarities of the charge transport through a given SMC can be explained in terms of the renormalized molecular levels (RMLs).[15] In a nutshell, after the self-consistent iteration of the Kohn-Sham equation is converged, the Hamiltonian matrix $H_{\mu\nu}$ is obtained. Then, the submatrix of the Hamiltonian associated with the atomic orbitals in the molecular structure of interest is diagonalized to produce RMLs. The energy spectrum obtained in this way is derived from a molecule interacting with the electrodes, where all the details of its interaction with the electrodes is automatically included through the self-consistent solution of the Kohn-Sham equation. Given procedure generally gives a very good correspondence between the transmission peaks and the RMLs.[15]

Since alkanes are poor conductors with a large HOMO-LUMO gap,[9,20,27,31] details of the transmission spectra within the HOMO-LUMO gap are governed by the additional states[9,48] arising in the HOMO-LUMO gap due to the coupling with the electrodes. The effect of these states on charge transport through SMCs is qualitatively equivalent to the ef-

fect of impurity states,[49] and, under finite bias, they can lead to a variety of observable effects in the *I-V* curves of SMCs.[49] Having their origin in the termination of an infinite electrode with a molecular junction, these additional states can also be associated with the surface states[50] of the molecular junction.

The RMLs levels computed by diagonalizing the sub-Hamiltonian which includes all the atoms in the scattering region [Fig. 1(B)] are shown in Figs. 3(A)–3(C) as solid triangles. For our analysis we have opted to use configurations 04, 13, and 15 as representatives of all the HC and LC quartets. As we have checked, RMLs of other configurations within each quartet are located very close to the corresponding RMLs of our chosen configurations.

As one can see in Fig. 3(A) for the HC quartet the value of the zero-bias conductance is defined by a wide tail of the resonance located near the Fermi energy, while for the LC quartets tunneling is nonresonant. The transmission spectrum of the configuration 04 [Fig. 3(A)] has three distinguishable peaks located at $E=-0.22$, -0.1, and -0.03 eV. The peak responsible for the conductance value is located at $E=-0.03$ eV and has six RMLs around it. To reveal the contribution from these levels we have calculated scattering states $\phi^{SS}(E)$ for energies between -0.06 and 0.1 eV and projected them onto the eigenstates φ_i^{RML} of the sub-Hamiltonian which includes all the atoms in the scattering region. The projection coefficient $P_i=|\langle\varphi_i^{\mathrm{RML}}|\phi^{SS}\rangle|^2$ shows the relative contribution of a given RML into the scattering state.

We found that contribution of these six RMLs to ϕ^{SS} is around 53%, while the contribution of all RMLs shown in Fig. 3(A) to the scattering-state wave function is around 92%. Among these six RMLs around E_f, the three that give the maximum projection coefficient are mainly composed of *s*, *p*, and *d* orbitals localized on Au atoms in the left part of the scattering region; the other three levels whose contribution is two orders of magnitude smaller are mainly composed of the orbitals localized on Au atoms in the right part of the scattering region. This proves our suggestion drawn from Fig. 4 that the origin behind the HC/LC separation is associated with the left electrode.

On the contrary, configuration 15 has only one RML in the vicinity of E_f with its 10% relative contribution to ϕ^{SS}, while the contribution of all RMLs shown in Fig. 3(C) is around 88%. Configuration 13 has two RMLs located in the vicinity of E_f, with the contribution of the state at energy $E<E_f$ being around 20%, and the state at energy $E>E_f$ having negligible contribution to ϕ^{SS}, while the contribution of all levels shown in Fig. 3(B) to the scattering-state wave function is around 78%.

Abundance of well coupled to ϕ^{SS} RMLs around some peaks leads to significant broadening of the transmission peaks. In other words, broader transmission peaks correspond to a more spatially delocalized scattering-state wave function, effectively leading to a shorter tunneling distance.[28] This goes in line with Ref. 16, where it is stated that the broadness of the transmission peaks arises due to the contribution from closely located states well coupled with the electrodes and different binding geometries, in which number of states coupled with the electrodes varies, might have narrower/broader transmission peaks depending on a number of the coupled states.

The quartetlike grouping of the transmission spectra [Figs. 3(A)–3(C)] can be understood in terms of the symmetry of the electrodes. Let us represent the stacking of the two-probe system as $\ldots \mathrm{A}n_2^l\mathbf{n}_3^l\mathbf{A}\mathbf{n}_2^ln_3^l$-Mol-$\tilde{\mathbf{n}}\mathbf{A}\mathbf{n}_2^rn_3^r\mathrm{A}\ldots$, where $\tilde{n}$ slice has the same *x* and *y* coordinates as n_3^l but is shifted onto L_c along *z* direction, $n_i^l=n_i^r$, $i=2,3$, and shown in bold are the slices taken to form the unit cell of the electrodes. Consider the left part of the scattering region that follows $\mathrm{A}n_2^ln_3^l$ stacking. Thus, configuration 13(24) is a mirror reflection (in a plane parallel to *z* axis) of 53(42). Going in the opposite direction *from the right to the left electrode*, it is easy to see that the part $\tilde{n}\mathrm{A}n_2^r$, which follows 13 *from-left-to-right* stacking, is now nothing but 42 configuration. Thus the quartetlike grouping of the transmission spectra is solely due to our choice $n_i^l=n_i^r$. Boundary conditions imposed on the Hartree potential by this direction-reversal symmetry to match it in the interfaces between the scattering region and the left and the right electrodes would give, as a result of the solution of the Kohn-Sham equations, a symmetric electron-density distribution that in turn results into the aforementioned grouping of the transmission spectra. Attached molecule breaks the symmetry, but with the main contribution to the conductance coming from the orbitals localized on Au atoms, the contribution from the orbitals localized on the molecule and the end groups results only in a small variations between the conductance spectra. Similar arguments apply to the other two quartets, Figs. 3(A) and 3(C).

Given a random distribution of the dozen stable configurations [Figs. 3(A)–3(C)] with four of them forming the high-conductance SMCs and eight other forming the low-conductance SMCs, probability of acquiring an HC set is about 33%, and probability of acquiring an LC set is correspondingly 67%, very close to the reported 34% and 58%,[23] correspondingly. To prove that a molecular binding site does not significantly influence the conducting character of our SMCs, we have calculated the conductance of junctions with configurations 04, 13, and 15 for a less energetically favorable configurations with a molecule bound (through the Au adatoms) within triangles (α) and (β), see Fig. 1(A), and found that configuration 04 for α/β binding sites still represents HC junction, while configurations 13 and 15 correspond to LC junction (however, the HC/LC separation in this case is smaller than that shown in Fig. 5). The experimental situation when in one single measurement both the HC and LC steps appear can find its explanation in the following reasoning: total energy of the scattering region for the LC quartets shown in Figs. 3(B) and 3(C) is around 1.5 eV lower than that of the HC quartet, Fig. 3(A). Thus, an initially HC SMC can relax into a more stable LC configuration during the junction stretching. This does provide an explanation why in experiments[23] HC steps always appear before LC steps, but never in reverse order.

Anther interesting question is whether the results reported here are universal with respect to the choice of the end groups and the cross-sectional area of the electrodes. To check that we have used enlarged Au(111) electrodes with (3×3) cross-section as shown in Fig. 1(A) and calculated conductance for a butane SMC for configurations 04 and 40 for the molecular binding site located within the $\otimes$-marked triangle, Fig. 1(A). The calculated conductance values (in

units of $G_0 \times 10^{-4}$, for the interelectrode distance $L = 21.1$ Å) are 0.815 for 04 [cf. with 15.59 for (2×2) cross-section] and 2.53 for 40 [0.468 for (2×2) cross-section] configurations, respectively. Changing the geometry of the electrodes varies their electronic structure;[51] since, in the case of poorly conducting ADTC molecules, conducting properties of the SMCs are mainly determined by the electrode part, this results in a drastic change in their transport properties. Thus, care should be taken with an explanation of the experimental results, since, as noted in Ref. 9, the contact area of an Au tip in a typical experiment is sufficiently large.

Having changed diisothiocyanate end groups for dithiol ones, we have also studied the end-group effects on the HC/LC separation. Once again, an alkane molecule with a thiol end group and one Au adatom from each side was placed between two (2×2) slices and the structure was relaxed in the same way as for the ADTC contacts.[52] Results for a hexane dithiol SMC (shown in the inset in Fig. 2) together with the numerical results of Müller[27] for a number of various atomic configurations of the molecule-electrode interface show a rather smooth distribution of the conductance values for the stable configurations of the electrodes with the unstable configurations (n_i, n_i) giving the main deviation,[53] suggesting that the effect of the electrode conformation (for the given binding site) on the transport properties of dithiol SMCs is much less pronounced. However, if the proper binding site of the molecular end groups is found through the unrestricted geometry relaxation, the effect of the electrode conformation on the transmission spectra can also be more pronounced in SMCs with dithiol and other molecular end groups.

Grouping of the transmission and the DOS spectra similar to that shown in Figs. 3(A)–3(E) is still preserved for the dithiole SMCs, however, deviations between the transmission spectra within each of the quartets in the group III are much larger than those within the corresponding quartets of the ADTC SMCs. The origin of the larger deviations in this case can be tracked down to the conclusion derived in Ref. 9 that RMLs associated with the sulfur atoms are located within the HOMO-LUMO gap of alkanes and play in case of alkanethiols a more important role in modifying their conduction properties. The interaction of the S atoms with the nearest variously stacked Au slices[38] gives larger deviations between the corresponding conductance spectra than in the case of ADTC junctions, where the role of RMLs associated with the sulfur atoms is minor.

IV. CONCLUSIONS

We have performed a detailed *ab initio* quantum-mechanical study of zero-bias transport properties of a number of alkanediisothiocyanate single-molecule contacts formed between two semi-infinite Au(111) electrodes with a finite cross-section. We have shown that the HC and LC conductance traces observed experimentally in these SMCs (Ref. 23) can be clearly reproduced in our numerical simulations for a single given binding site of an ADTC molecule, contrary to the usual explanation of the HC/LC traces for the thiol-terminated SMCs that assumes different geometries of the sulfur-gold binding.[20,21,27] What matters in the case of poorly conducting ADTCs is the electronic structure of the combined molecule and electrodes system, the metal-molecule-metal junction, which is defined by how the electrodes form the scattering region. Some configurations have a number of well coupled to the scattering-state wave function RMLs around the Fermi energy—these contacts represent the HC SMCs; other configurations with sparser distribution of RMLs around E_f represent the LC SMCs. The RMLs that are responsible for the conductance enhancement are mainly composed of the atomic orbitals of the Au atoms located near the molecule-electrode interface, and thus can be identified as the surface states of the junctions.

The major unknowns of every experimental system are the exact geometry of SMCs, nature of the bond between the molecule and the electrodes and the actual interelectrode separation (length of an SMC). Moreover, since the experimental data usually come from statistical averaging of typically thousands of conductance measurements, it is not surprising that numerical results obtained for any given SMC configuration may not be in good quantitative agreement with experiments.[11] In order to obtain a more quantitative theoretical estimate for the relative probability of each of the configurations of the molecular contacts, a time-consuming realistic statistical analysis on the structural changes (those include, to name a few, interelectrode distance, binding geometry, molecular orientation, electrode structure, etc.) at the molecule-electrode contacts is required,[54] but the results reported in the present study should nevertheless represent characteristic trends.

*luzhbin@imp.kiev.ua
†kauncc@gate.sinica.edu.tw

[1] N. J. Tao, Nat. Nanotechnol. **1**, 173 (2006).
[2] B. Xu and N. J. Tao, Science **301**, 1221 (2003).
[3] R. L. McCreery, Chem. Mater. **16**, 4477 (2004).
[4] J. Taylor, H. Guo, and J. Wang, Phys. Rev. B **63**, 245407 (2001); J. Taylor, Ph.D. thesis, McGill University, 2000.
[5] M. Brandbyge, J. L. Mozos, P. Ordejón, J. Taylor, and K. Stokbro, Phys. Rev. B **65**, 165401 (2002).
[6] Y. Xue, S. Datta, and M. A. Ratner, Chem. Phys. **281**, 151 (2002).
[7] W. Y. Kim and K. S. Kim, J. Comput. Chem. **29**, 1073 (2008).
[8] M. A. Ratner, Mater. Today **5**, 20 (2002); C. Joachim and M. A. Ratner, Proc. Natl. Acad. Sci. U.S.A. **102**, 8801 (2005).
[9] C.-C. Kaun and H. Guo, Nano Lett. **3**, 1521 (2003).
[10] C.-C. Kaun, B. Larade, and H. Guo, Phys. Rev. B **67**, 121411(R) (2003).
[11] S. M. Lindsay and M. A. Ratner, Adv. Mater. (Weinheim, Ger.) **19**, 23 (2007).
[12] D. Waldron, P. Haney, B. Larade, A. MacDonald, and H. Guo, Phys. Rev. Lett. **96**, 166804 (2006); D. Waldron, V. Timoshevskii, Y. Hu, K. Xia, and H. Guo, *ibid.* **97**, 226802 (2006); Z.

Ning, Y. Zhu, J. Wang, and H. Guo, *ibid.* **100**, 056803 (2008).
[13] C. Roland, V. Meunier, B. Larade, and H. Guo, Phys. Rev. B **66**, 035332 (2002).
[14] B. Larade, J. Taylor, H. Mehrez, and H. Guo, Phys. Rev. B **64**, 075420 (2001); J. Taylor, H. Guo, and J. Wang, *ibid.* **63**, 121104(R) (2001).
[15] B. Larade, J. Taylor, Q. R. Zheng, H. Mehrez, P. Pomorski, and H. Guo, Phys. Rev. B **64**, 195402 (2001).
[16] K. Stokbro, J. Taylor, M. Brandbyge, J. L. Mozos, and P. Ordejón, Comput. Mater. Sci. **27**, 151 (2003).
[17] H. Basch, R. Cohen, and M. A. Ratner, Nano Lett. **5**, 1668 (2005).
[18] Z. Huang, F. Chen, P. A. Bennett, and N. Tao, J. Am. Chem. Soc. **129**, 13225 (2007).
[19] I.-W. P. Chen, M.-D. Fu, W.-H. Tseng, J.-Y. Yu, S.-H. Wu, C.-J. Ku, C.-H. Chen, and S.-M. Peng, Angew. Chem., Int. Ed. **45**, 5814 (2006).
[20] C. Li, I. Pobelov, T. Wandlowski, A. Bagrets, A. Arnold, and F. Evers, J. Am. Chem. Soc. **130**, 318 (2008).
[21] X. Li, J. He, J. Hihath, B. Xu, S. M. Lindsay, and N. Tao, J. Am. Chem. Soc. **128**, 2135 (2006).
[22] F. Chen, X. Li, J. Hihath, Z. Huang, and N. J. Tao, J. Am. Chem. Soc. **128**, 15874 (2006).
[23] M.-D. Fu, I.-W. P. Chen, H.-C. Lu, C.-T. Kuo, W.-H. Tseng, and C.-H. Chen, J. Phys. Chem. C **111**, 11450 (2007).
[24] A. M. Moore, A. A. Dameron, B. A. Mantooth, R. K. Smith, D. J. Fuchs, J. W. Ciszek, F. Maya, Y. Yao, J. M. Tour, and P. S. Weiss, J. Am. Chem. Soc. **128**, 1959 (2006).
[25] A. Grigoriev, J. Sköldberg, G. Wendin, and Ž. Crljen, Phys. Rev. B **74**, 045401 (2006).
[26] W. Wang, T. Lee, and M. A. Reed, J. Phys. Chem. B **108**, 18398 (2004).
[27] K.-H. Müller, Phys. Rev. B **73**, 045403 (2006).
[28] C.-C. Kaun and T. Seideman, Phys. Rev. B **77**, 033414 (2008).
[29] J. M. Seminario, C. E. De La Cruz, and P. A. Derosa, J. Am. Chem. Soc. **123**, 5616 (2001); J. M. Seminario, A. G. Zacarias, and J. M. Tour, *ibid.* **121**, 411 (1999); H. Kondo, J. Nara, H. Kino, and T. Ohno, Jpn. J. Appl. Phys. **47**, 4792 (2008); Y. Xue and M. A. Ratner, Phys. Rev. B **69**, 085403 (2004).
[30] G. Fagas and J. C. Greer, Nanotechnology **18**, 424010 (2007).
[31] S. McDermott, C. B. George, G. Fagas, J. C. Greer, and M. A. Ratner, J. Phys. Chem. C **113**, 744 (2009).
[32] Y. S. Park, A. C. Whalley, M. Kamenetska, M. L. Steigerwald, M. S. Hybertsen, C. Nuckolls, and L. Venkataraman, J. Am. Chem. Soc. **129**, 15768 (2007).
[33] L. Venkataraman, J. E. Klare, I. W. Tam, C. Nuckolls, M. S. Hybertsen, and M. L. Steigerwald, Nano Lett. **6**, 458 (2006).
[34] X. Li and A. Gewirth, J. Am. Chem. Soc. **125**, 11674 (2003).
[35] C. Vericat, M. E. Vela, G. A. Benitez, J. A. Martin Gago, X. Torrelles, and R. C. Salvarezza, J. Phys.: Condens. Matter **18**, R867 (2006); A. Ulman, J. E. Eilers, and N. Tillman, Langmuir **5**, 1147 (1989).
[36] J. He, O. Sankey, M. Lee, N. J. Tao, X. Li, and S. Lindsay, Faraday Discuss. **131**, 145 (2006).
[37] Q. Pu, Y. Leng, L. Tsetseris, H. S. Park, S. T. Pantelides, and P. T. Cummings, J. Chem. Phys. **126**, 144707 (2007); M. Dreher, F. Pauly, J. Heurich, J. C. Cuevas, E. Scheer, and P. Nielaba, Phys. Rev. B **72**, 075435 (2005).
[38] H. Sellers, A. Ulman, Y. Shnidman, and J. E. Eilers, J. Am. Chem. Soc. **115**, 9389 (1993).
[39] C. Vericat, M. E. Vela, and R. C. Salvarezza, Phys. Chem. Chem. Phys. **7**, 3258 (2005); L.-J. Wan, M. Terashima, H. Noda, and M. Osawa, J. Phys. Chem. B **104**, 3563 (2000); Z.-Y. Yang, H.-M. Zhang, C.-J. Yan, S.-S. Li, H.-J. Yan, W.-G. Song, and L.-J. Wan, Proc. Natl. Acad. Sci. U.S.A. **104**, 3707 (2007).
[40] M. J. Frisch, G. W. Trucks, H. B. Schlegel, G. E. Scuseria, M. A. Robb, J. R. Cheeseman, J. A. Montgomery, Jr., T. Vreven, K. N. Kudin, J. C. Burant, J. M. Millam, S. S. Iyengar, J. Tomasi, V. Barone, B. Mennucci, M. Cossi, G. Scalmani, N. Rega, G. A. Petersson, H. Nakatsuji, M. Hada, M. Ehara, K. Toyota, R. Fukuda, J. Hasegawa, M. Ishida, T. Nakajima, Y. Honda, O. Kitao, H. Nakai, M. Klene, X. Li, J. E. Knox, H. P. Hratchian, J. B. Cross, V. Bakken, C. Adamo, J. Jaramillo, R. Gomperts, R. E. Stratmann, O. Yazyev, A. J. Austin, R. Cammi, C. Pomelli, J. W. Ochterski, P. Y. Ayala, K. Morokuma, G. A. Voth, P. Salvador, J. J. Dannenberg, V. G. Zakrzewski, S. Dapprich, A. D. Daniels, M. C. Strain, O. Farkas, D. K. Malick, A. D. Rabuck, K. Raghavachari, J. B. Foresman, J. V. Ortiz, Q. Cui, A. G. Baboul, S. Clifford, J. Cioslowski, B. B. Stefanov, G. Liu, A. Liashenko, P. Piskorz, I. Komaromi, R. L. Martin, D. J. Fox, T. Keith, M. A. Al-Laham, C. Y. Peng, A. Nanayakkara, M. Challacombe, P. M. W. Gill, B. Johnson, W. Chen, M. W. Wong, C. Gonzalez, and J. A. Pople, GAUSSIAN 03, Revision D.02, Gaussian, Inc., Wallingford CT, 2004.
[41] Ž. Crljen, A. Grigoriev, G. Wendin, and K. Stokbro, Phys. Rev. B **71**, 165316 (2005).
[42] D. R. Hamann, M. Schlüter, and C. Chiang, Phys. Rev. Lett. **43**, 1494 (1979).
[43] J. P. Perdew and A. Zunger, Phys. Rev. B **23**, 5048 (1981).
[44] J. P. Perdew, K. Burke, and M. Ernzerhof, Phys. Rev. Lett. **77**, 3865 (1996).
[45] The junction breakage length L_c is estimated visually using the default settings of Molden, see G. Schaftenaar and J. H. Noordik, J. Comput.-Aided Mol. Des. **14**, 123 (2000). The breakage occurs between the S atom and the Au adatom from the right side.
[46] M. Brandbyge, N. Kobayashi, and M. Tsukada, Phys. Rev. B **60**, 17064 (1999); J. C. Cuevas, A. Levy Yeyati, and A. Martín-Rodero, Phys. Rev. Lett. **80**, 1066 (1998); D. Jacob and J. J. Palacios, Phys. Rev. B **73**, 075429 (2006).
[47] M. Paulsson and M. Brandbyge, Phys. Rev. B **76**, 115117 (2007).
[48] C. Zeng, B. Li, B. Wang, H. Wang, K. Wang, J. Yang, J. G. Hou, and Q. Zhu, J. Chem. Phys. **117**, 851 (2002).
[49] B. Larade and A. M. Bratkovsky, Phys. Rev. B **72**, 035440 (2005).
[50] E. A. Pashitskii and A. E. Pashitskii, JETP Lett. **60**, 35 (1994).
[51] J. G. Wang, E. Prodan, R. Car, and A. Selloni, Phys. Rev. B **77**, 245443 (2008).
[52] We found that for the dithiol junctions ⊗-marked binding site is extremely unstable and during the relaxation all molecules moved toward the edge of the slices forming a kind of a gauche conformation reported in Ref. 20 (this is in contrast with the cases reported in Refs. 9 and 17, where alkanedithiols were optimized as either isolated molecules or with Au atoms terminating the S atoms and put afterwards rather arbitrarily in between the electrodes). However, by suitable choice of the initial geometry and using "steep" option (Ref. 40) for geometry relaxation, for certain interelectrode distances L it is possible to converge the system to a local energy minimum with the Au adatoms bound within the ⊗-marked triangles.

[53] The discrepancy between our numerical results and those of Müller (Ref. 27) is due to two factors: (i) different electrodes used in the calculations: one dimensional in our case and bulk in Müller's and (ii) different terminal atomic configurations. Note that the conductance of the junction with terminal configuation numbered (5) in Ref. 27, which is the same as the one used in the present work, is very close to the values obtained in our calculations, see inset in Fig. 2.

[54] Y. Hu, Y. Zhu, H. Gao, and H. Guo, Phys. Rev. Lett. **95**, 156803 (2005).